Analysis of Electric Field Distribution Induced by 50Hz Magnetic Fields Utilizing Fast-multipole Surface-charge-simulation Method for Voxel Models

AUTHOR(S):

Hamada, S.; Kobayashi, T.

The International Conference of Computational Methods
April 4-6, 2007, Hiroshima

ANALYSIS OF ELECTRIC FIELD DISTRIBUTION INDUCED BY 50Hz MAGNETIC FIELDS UTILIZING FAST-MULTIPOLE SURFACE-CHARGE-SIMULATION METHOD FOR VOXEL MODELS

S. Hamada, T. Kobayashi
Department of Electrical Engineering
Kyoto University, Kyotodaigaku-Katsura, Nishikyo-ku, Kyoto 615-8510, JAPAN
shamada@kuee.kyoto-u.ac.jp; tetsuo@kuee.kyoto-u.ac.jp

Abstract

This paper applies the diagonal form Fast-Multipole Method (FMM; Greengard, 1997) to the Surface-Charge-simulation Method (SCM) for voxel models. This method is used here to analyze electric field distribution induced by 50Hz magnetic fields. The SCM for voxel models treats the square surface of a voxel that has different inside and outside conductivities as a surface element of the SCM that calculates a three-dimensional Laplacian field. SCM is sometimes called the indirect-Boundary Element Method (BEM) or is considered a kind of Methods of Moment (MoM) approach. The performance of the combined FMM-SCM for voxel models approach was demonstrated by calculating the induced electric fields in a whole body model for a Japanese adult male composed of 7,977,906, 2x2x2mm^3 voxels.

Keywords: Electric field, Magnetic field, Voxel, Surface-Charge-simulation Method

Introduction

A variety of numerical methods are used to calculate magnetically induced electric fields in realistic high-resolution human voxel models. The most popular methods, such as the Scalar Potential Finite-Difference method (SPFD), the Finite-Difference Time-Domain method (FDTD), the Finite Element Method (FEM), etc. require O(D^3) memory-capacity and operation-cost, when the number of voxels is roughly D^3. Although this is superior to the O($D^{4\text{-}6}$) costs of the conventional BEM, SCM, and MoM, an increase in the size of D continues to cause an intolerable cost increase. In order to overcome this problem, we had proposed FMM-SCM for voxel models in previous work (Hamada, 2006a, 2006b). This method treats a square surface of a cubic voxel that has different inside and outside conductivities as a surface element of an SCM that calculates a three-dimensional Laplacian field. The main features of the method are as follows. (I) The diagonal form FMM provides O(D^2) performance in memory-capacity and operation-cost, when the number of voxels is approximately D^3. (II) The boundary equation integrated over each element strictly imposes flux continuity, therefore the solution globally satisfies Gauss'

law. These features make this a high-speed, high-capacity, and high-stability calculation method.

Basic Equations

The basic equations that describe magnetically induced, low frequency, faint currents in a human body are described in a great deal of existing work (Dawson, 1997). By neglecting the effect of permittivity, the induced electric field $\boldsymbol{E}$ and the current density $\boldsymbol{J}$ satisfy the following equations.

$$\boldsymbol{E} = -\mathrm{j}\omega\{\boldsymbol{A} + \nabla\phi\} \quad , \quad \boldsymbol{J} = \sigma\boldsymbol{E} \quad , \quad \nabla^2\phi = 0 \tag{1}$$

where j, ω, $\boldsymbol{A}$, $\boldsymbol{J}$, σ, and ϕ are: imaginary units, the angular frequency, the given vector potential equivalent to the applied magnetic field, the current density, the conductivity, and the unknown scalar potential, respectively. The boundary equations are as follows.

$$\sigma_1\{\boldsymbol{A} + \nabla\phi_1\} \cdot \boldsymbol{n} = \sigma_2\{\boldsymbol{A} + \nabla\phi_2\} \cdot \boldsymbol{n} \quad , \quad \phi_1 = \phi_2 \tag{2}$$

where subscripts 1 and 2 denote both sides of the boundary surface, and $\boldsymbol{n}$ is the unit normal vector on the surface. SCM by definition satisfies the latter equation of Eq. (2). Thus it explicitly treats the former in the following surface-integrated form.

$$\sigma_1 \int_{S_i} \nabla\phi_1 \cdot \boldsymbol{n} dS - \sigma_2 \int_{S_i} \nabla\phi_2 \cdot \boldsymbol{n} dS = -(\sigma_1 - \sigma_2) \int_{S_i} \boldsymbol{A} \cdot \boldsymbol{n} dS \quad , \quad i = 1 \sim N \tag{3}$$

where S is the square surface of each element, subscript i denotes element number, and N is the number of elements. This equation describes the continuity of flux flowing through the i-th element. SCM expresses ϕ and $\nabla\phi$ by superimposing the Laplacian fields generated by surface elements that have the equivalent surface charges. The uniform charge density x_i on the i-th element can be determined by solving a linear system that is equivalent to the boundary equations (3) with an iterative solver, such as Bi-CGSTAB2 (Gutknecht, 1993).

Interface with FMM

Diagonal form FMM (Greengard, 1997) was used to speed up the solver, by defining a cubic voxel-cluster, for example 5x5x5 voxels, as the leaf-cell of a three-dimensional octal-tree structure. FMM calculates the left hand side of Eq. (3) as the summation of the "near" part and the "far" part contributions. The near part contribution of x_j is calculated by the following equation.

$$\left(\int_{S_i} \nabla\phi \cdot \boldsymbol{n} dS\right)^{\mathrm{near}} = \sum_{j \text{ in near}} x_j \alpha_j^{\mathrm{rel}} \tag{4}$$

where "j in near" represents accumulating direct contribution from the j-th elements belonging to the following leaf-cells; (i) the leaf-cell containing the i-th element and (ii) the near leaf-cells surrounding (i). The proportional constants α_j^{rel} are preliminarily

calculated and stored in an array whose elements indicate the relative location of the *j*-th element from the *i*-th element.

The far part contribution of x_j is calculated by the following processes. The field contribution by x_j in a leaf-cell is translated into the multipole-expansion coefficients leaf-M_n^m defined on the leaf-cell by the following equation.

$$\text{leaf-}M_n^m = \sum_{j \text{ in leaf}} x_j (\beta_n^m)_j^{\text{rel}} \tag{5}$$

where "*j* in leaf" stands for accumulating contribution from the *j*-th elements belonging to the leaf-cell. The proportional complex constants $(\beta_n^m)_j^{\text{rel}}$ are preliminarily calculated and stored in an array whose elements indicate the relative location of the *j*-th element in the leaf-cell. After calculating all the local-expansion coefficients leaf-L_n^m defined on leaf-cells from the leaf-M_n^m using the diagonal form FMM algorithm, the far part contribution for the *i*-th element is calculated by the following equation.

$$\left(\int_{S_i} \nabla\phi \cdot \boldsymbol{n} dS\right)^{\text{far}} = \sum_{k=1}^{(p+1)^2} (\{\text{Re/Im}\} \text{ leaf-}L_n^m)_k \gamma_k^{\text{rel}} \tag{6}$$

where *p* is the maximum value of *n*, {Re/Im} is the real or imaginary part of the complex number L_n^m. The proportional constants γ_k^{rel} are preliminarily calculated and stored in an array whose elements indicate the relative location of the *i*-th element in the leaf-cell. The preliminarily calculated coefficients α_j^{rel}, $(\beta_n^m)_j^{\text{rel}}$, and γ_k^{rel} contain numerical area integration over the element surface *S*. This preliminary calculation is key as it skips costly numerical integration during each iteration step of the iterative solver. The memory capacity required for storing these coefficients is only several Mbytes owing to the small number of relative locations, at most several hundred thousand, because they are restricted to the leaf cell or to the near region defined for the FMM.

Determining the Field at the Voxel Center and Field Smoothing near Boundaries

After solving the surface charge densities x_i (*i*=1-*N*), we can calculate $\int_S \boldsymbol{E} \cdot \boldsymbol{n} dS$ on the six inner surfaces of each voxel, which are denoted by f^{x+}, f^{x-}, f^{y+}, f^{y-}, f^{z+}, and f^{z-}. They yield a representative field at the center of a voxel as follows.

$$\boldsymbol{E}^{\text{center}} \equiv \frac{f^{\text{x}+} + f^{\text{x}-}}{2S}\boldsymbol{i} + \frac{f^{\text{y}+} + f^{\text{y}-}}{2S}\boldsymbol{j} + \frac{f^{\text{z}+} + f^{\text{z}-}}{2S}\boldsymbol{k} \tag{7}$$

where *S* is the area of one surface of the voxel. It has been shown that $\boldsymbol{E}^{\text{center}}$ represents induced fields with good accuracy except for those in the vicinity of the boundary (Hamada, 2006a). Sharp fluctuations in $\boldsymbol{E}^{\text{center}}$ were observed in the vicinity of the boundary owing to the lack of exact information on the boundary shape. This was caused by staircase shape approximation of the voxels. This is a common problem shared by voxel model based field calculation methods.

In this paper, a smoothing process is added for $\boldsymbol{E}^{\text{center}}$ in regions near boundaries. First, a weight value w_6 ($0 \leqq w_6 \leqq 6$) corresponding to the number of own voxel surfaces not

treated as boundary surface elements is set for each voxel. This means that the smaller the weight is, the closer the boundary. Second, another weight value w_{162} ($0 \leqq w_{162} \leqq 162$) is set for each voxel. The w_{162} for a treated-voxel corresponds to the sum of the w_6 values for the voxels satisfying both (a) they are among the 3x3x3-1 voxels surrounding the treated-voxel, or the treated-voxel itself, and (b) they have the same conductivity as the treated-voxel. Third, when w_{162} is neither 0 nor 162, we replace the $\boldsymbol{E}^{\text{center}}$ of the voxel by the following weighted average value.

$$\boldsymbol{E}^{\text{center}}_{\text{replaced}} = \frac{\sum_\ell w_{6\ell} \boldsymbol{E}^{\text{center}}_\ell}{w_{162}} \ , \quad w_{162} = \sum_\ell w_{6\ell} \tag{8}$$

Where $\sum_\ell$ represents accumulating the values for the voxels satisfying both the above mentioned rules (a) and (b). This procedure is called 'near boundary smoothing'. It should be noted that such smoothing procedures can be designed in various ways, and that this procedure is simply one practical example.

NICT Taro Model and Applied Fields

Taro is a whole body model of an adult Japanese male. Taro was developed by the National Institute of Information and Communications Technology (NICT), Kitasato Univ., Keio Univ., and Tokyo Metropolitan University (Nagaoka, 2004). Taro, excluding the surrounding air, consists of 7,977,906 voxels, and the cubic voxel size is 2mm. Taro occupies a space of 0mm–516mm in the *x*, 0mm–270mm in the *y*, and 0mm–1732mm in the *z*-axis. Taro's gravity center is located (251.5, 122.5, 959.5) in mm. Taro's tissue, conductivity, and the corresponding number of voxels is listed in Table 1. We can determine the location of surface elements based on this data, and their number to be 3,921,953. A 50Hz homogeneous magnetic field was applied to Taro. The applied fields is $B\boldsymbol{i}$ (left-to-right), $B\boldsymbol{j}$ (back-to-front), and $B\boldsymbol{k}$ (foot-to-head), where B=1μT (peak).

Results and Discussions

The parameter settings for the FMM are as follows. A 5x5x5 voxel-cluster defines a leaf-cell. The maximum degree of the multipole and local expansions, *p,* is ten. The maximum order of exponential expansion for diagonal translation (Greengard, 1997) is eighteen. An additional condition of total-surface-charge being zero regularizes the linear system matrix equivalent to Eq. (3). The iterative solver Bi-CGSTAB2 reduces the relative residual norms to less than 10^{-7}.

Fig. 1 (i) shows an example of the convergence of residual norms when $B\boldsymbol{k}$ is applied. Fig. 1(ii) shows required calculation times per FMM operation, where "M to M", "M to L", and "L to L" stand for translation operations between multipole and local coefficients. Fig. 1(ii) shows that "Eq. (4)" and "M to L" processes occupied about 94 percent of the FMM operation time. In these processes, each element required about 1650 entries on average for the summation in Eq. (4). The number of all cells, and leaf-cells, was 78375, and 65222, respectively, and each cell required about 125 "M to L" translations on average. It should be noted that each iterative step of Bi-CGSTAB2 required two FMM

operations. Table 2 shows the calculation times, number of iterative steps required, and electric field strength E (μVm^{-1}) for Taro's entire body. The script "max" and "ave" stand for maximum and average value, respectively. It was shown that the calculation times were about a hundred minutes in all cases. All calculations were carried out on a 2.66GHz, 3.3Gbyte-RAM, Core2Duo, Windows PC. The required memory capacity to run the code was 1.16Gbyte.

The left hand sides of Figs. 2-4 show the calculated electric field distributions induced by the $B\boldsymbol{i}$, $B\boldsymbol{j}$, and $B\boldsymbol{k}$, respectively, for a coronal slice at y=137mm, a sagittal slice at x=259mm, and horizontal slices at z=1599, 1325, 1051, 777, 503, and 229mm. The gradation from black to white corresponds to the field strength from $\log_{10}(0.01E_{\max}/\mu\text{Vm}^{-1})$ to $\log_{10}(E_{\max}/\mu\text{Vm}^{-1})$. The right hand sides of Figs. 2-4 show z-layer-maximum, z-layer-averaged, tissue-maximum, and tissue-averaged field strength (μVm^{-1}) before and after near boundary smoothing. It is observed that the smoothing process almost always reduces the maximum value, and doesn't change the average value significantly. The averaged values shown in Table 2 and Figs. 2-4 are qualitatively consistent with those in Dawson (1997) calculated by the SPFD method, the maximum values being relatively small in comparison owing to the smoothing procedure near boundaries.

Conclusions

The effectiveness of FMM (Fast-Multipole Method)-SCM (Surface-Charge-simulation Method) for voxel models was shown by calculating the induced electric fields in a Japanese adult male voxel model "Taro" licensed from NICT. Taro is composed of 7,977,906, 2x2x2mm^3 voxels, and was exposed to three kinds of homogeneous 50Hz magnetic fields. It was shown that the required calculation times were about a hundred minutes on a 2.66GHz, 3.3Gbyte-RAM, Core2Duo, Windows PC. These results demonstrated high-speed, high-capacity, and high-stability performance of the method.

Acknowledgements

This work was supported by grants-in-aid from Takahashi Industrial and Economic Research Foundation, and Japan Society for the Promotion of Science (JSPS).

References

T. W. Dawson, K. Caputa, and M. A. Stuchly (1997), Influence of human model resolution on computed currents induced in organs by 60-Hz magnetic fields, *Bioelectromagnetics*, 18, pp. 478-490.

L. Greengard and V. Rokhlin (1997), A new version of the fast multipole method for the Laplace equation in three dimensions, *Acta Numerica*, 6, pp. 229-269.

M. H. Gutknecht (1993), Variants of Bi-CGSTAB for matrices with complex spectrum, *SIAM J. Sci. Comput.*, 14, pp. 1020-1033.

S. Hamada, T. Kobayashi (2006a), Analysis of electric field induced by ELF magnetic field utilizing fast-multipole surface-charge-simulation method for voxel data, *IEEJ Trans. FM*, 126, No.5, pp.355-362.

S. Hamada, T. Kobayashi (2006b), Analysis of current density distribution induced by ELF magnetic fields utilizing fast-multipole surface-charge-simulation method for voxel data, Progress in Electromagnetics Research Symposium 2006-Tokyo, Japan, August 2-5 Session 4A2, pp.483-487.

T. Nagaoka, S. Watanabe, K. Sakurai, E. Kunieda, S. Watanabe, M. Taki, and Y. Yamanaka (2004), Development of realistic high-resolution whole-body voxel models of Japanese adult males and females of average height and weight, and application of models to radio-frequency electromagnetic-field dosimetry, *Phys. Med. Biol.* 49, pp. 1-15.

Table 1. Number of tissue, conductivity (Sm^{-1}), and voxels

No.	Tissue	σ	Voxels	No.	Tissue	σ	Voxels
1	Cerebellum	0.1	17320	30	Prostate	0.4	4053
2	CSF	2.0	54200	31	Small Intestine	0.5	40280
3	Cornea	0.4	25	32	Spleen	0.1	17206
5	Vitreous Humor	1.5	2124	33	Stomach	0.5	22925
6	Grey Matter	0.1	73362	34	Contents of 33	0.35	8766
7	Hypothalamus	0.08	77	35	Tendon	0.3	7045
8	Lens	0.25	73	36	Testis	0.35	14098
9	Pineal Glands	0.08	20	38	Thyroid, Thymus	0.5	1899
10	Pituitary	0.08	39	39	Trachea	0.35	3563
11	Salivary Gland	0.35	8271	40	Urine	0.7	40055
12	Thalamus	0.08	2967	44	Blood	0.7	148587
13	Tongue	0.3	11896	45	Cortical Bone	0.02	456228
14	White Matter	0.06	76094	46	Marrow	0.06	509507
15	Adrenals	0.35	247	47	Cartilage	0.18	33015
16	Bladder	0.2	7701	48	Fat (Mean)	0.04	1962602
18	Large Intestine	0.1	43411	49	Muscle (Mean)	0.35	3193078
19	Contents of 18	0.35	47188	50	Nerve	0.03	11340
20	Duodenum	0.5	1105	51	Skin	0.1	422953
21	Esophagus	0.5	860	52	Tooth	0.02	3112
22	Bile	1.4	944	53	Ligament	0.3	18268
23	Gall Bladder	0.2	548	54	Contents of 31	0.35	32270
24	Heart	0.1	50850	55	Diaphragm	0.35	7649
25	Kidney	0.1	37003	56	Seminal Vesicle	0.35	2739
26	Liver	0.07	143784	57	Cavernous Body	0.35	16268
27	Lung	0.014	412003				
29	Pancreas	0.35	8288		Whole Body		7977906

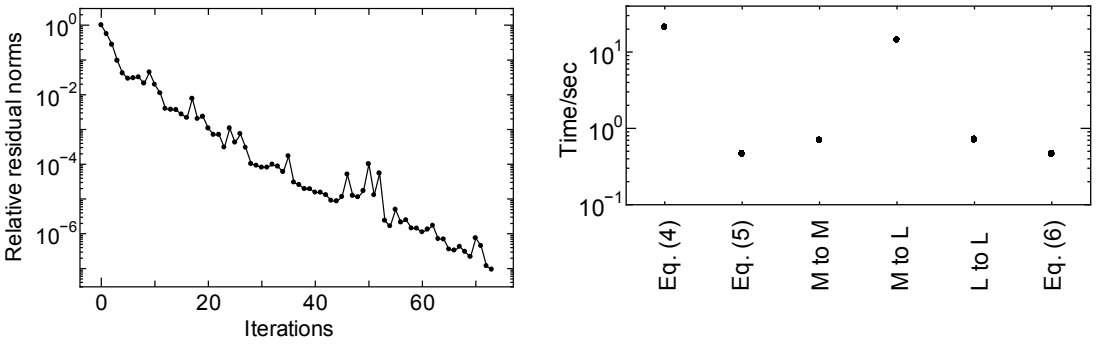

(i) Convergence of relative residual norms **(ii) Required time in each process**

Figure 1. Convergence properties and calculation time for each process

Table 2. Calculation times, iterations, and electric field strengths (μVm^{-1})

Case	Time	Iterations	Before smoothing		After smoothing	
			E_{max}	E_{ave}	E_{max}	E_{ave}
Bi (left-to-right)	100min. 15sec	74	198.8	11.2	147.0	11.1
Bj (back-to-front)	115min. 27sec	86	370.7	14.7	218.3	14.6
Bk (foot-to-head)	99min. 07sec	73	187.8	9.90	171.1	9.79

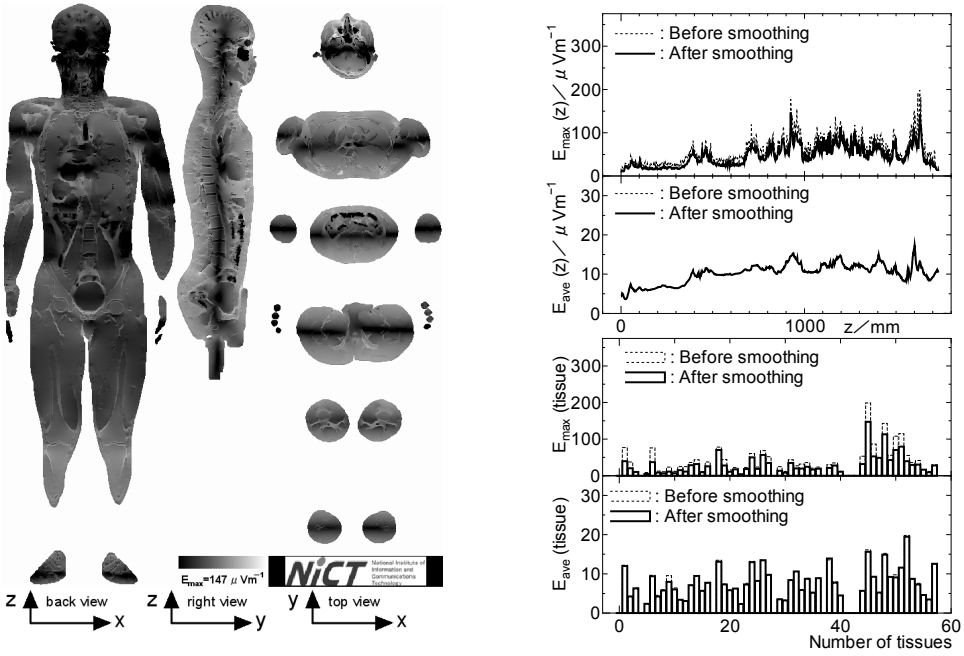

Figure 2. Electric field distributions and layer-maximum, layer-averaged, tissue-maximum, and tissue-averaged electric field strength (μVm^{-1}) induced by 1μT (peak), 50Hz, uniform *Bi* (left-to-right) magnetic fields

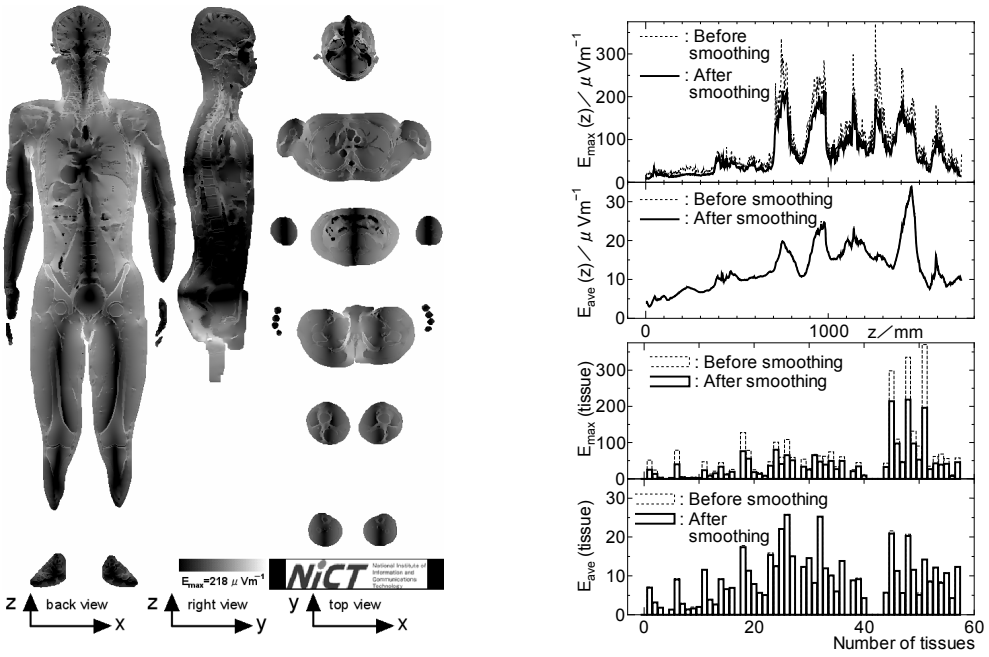

Figure 3. Electric field distributions and layer-maximum, layer-averaged, tissue-maximum, and tissue-averaged electric field strength (μVm^{-1}) induced by 1μT (peak), 50Hz, uniform *Bj* (back-to-front) magnetic fields

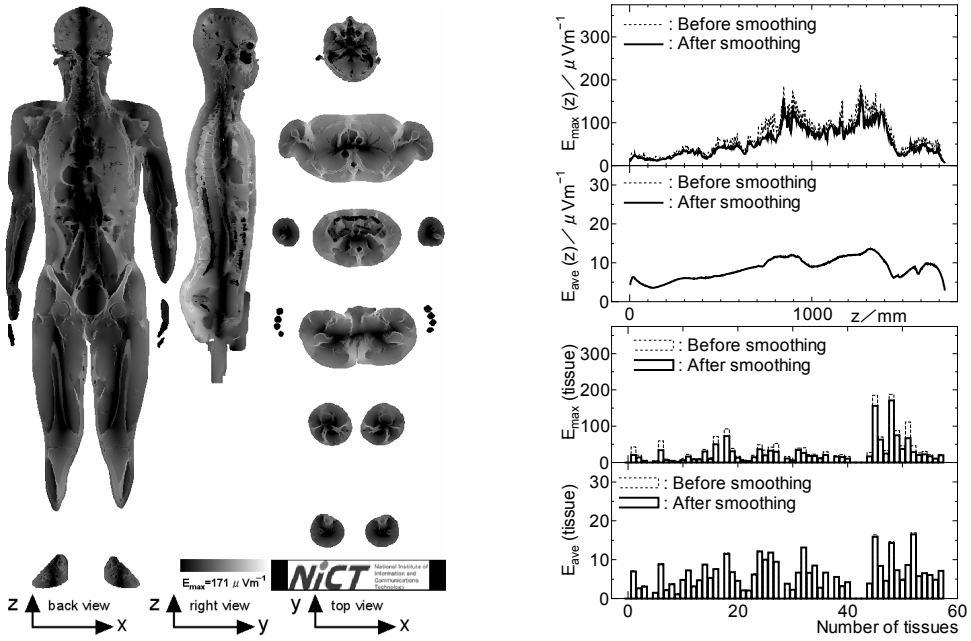

Figure 4. Electric field distributions and layer-maximum, layer-averaged, tissue-maximum, and tissue-averaged electric field strength (μVm^{-1}) induced by 1μT (peak), 50Hz, uniform *Bk* (foot-to-head) magnetic fields